Tin- and titanium-doped γ-$Fe_2O_3$ (maghemite)



2001 J. Phys.: Condens. Matter 13 10785

(http://iopscience.iop.org/0953-8984/13/48/305)

INSTITUTE OF PHYSICS PUBLISHING JOURNAL OF PHYSICS: CONDENSED MATTER

J. Phys.: Condens. Matter **13** (2001) 10785–10797 PII: S0953-8984(01)25783-X

# Tin- and titanium-doped $\gamma$-$Fe_2O_3$ (maghemite)

**Örn Helgason[1], Jean-Marc Greneche[2], Frank J Berry[3], Steen Mørup[4] and Frederick Mosselmans[5]**

[1] Science Institute, University of Iceland, Dunhagi 3, IS-107 Reykjavik, Iceland
[2] LPEC, UMR 6087, Université du Maine, 72085 Le Mans Cedex 9, France
[3] Department of Chemistry, The Open University, Walton Hall, Milton Keynes MK7 6AA, UK
[4] Department of Physics, Building 307, Technical University of Denmark, DK-2800 Kgs. Lyngby, Denmark
[5] CLRC Daresbury Laboratory, Daresbury, Warrington, WA4 4AD, UK

Received 14 June 2001, in final form 21 September 2001
Published 16 November 2001
Online at stacks.iop.org/JPhysCM/13/10785

**Abstract**

2.5% and 8% tin- and 8% titanium-doped $\gamma$-$Fe_2O_3$ have been synthesized and examined by x-ray powder diffraction, EXAFS, electron microscopy and by $^{57}$Fe- and $^{119}$Sn-Mössbauer spectroscopy. The Sn- and Ti-K-edge EXAFS show that both tin and titanium adopt octahedral sites in the spinel related $\gamma$-$Fe_2O_3$ structure. However, whereas tin substitutes for iron on one of the fully occupied sites, titanium adopts the octahedral site, which is only partially occupied. The $^{57}$Fe-Mössbauer spectra recorded in the presence of a longitudinal magnetic field of 2–8 T confirm that the tetravalent ions adopt the octahedral sites. The canting angles for both sublattices in $\gamma$-$Fe_2O_3$ were determined from the in-field Mössbauer spectra. The $^{119}$Sn-Mössbauer spectra showed that the maximum hyperfine field sensed by the $Sn^{4+}$ ions in $\gamma$-$Fe_2O_3$ is about 2/3 of that observed in tin-doped $Fe_3O_4$ (magnetite).

## 1. Introduction

The iron(III) oxide $\gamma$-$Fe_2O_3$, maghemite, adopts a spinel-related structure, commonly represented by the formula $(Fe)[Fe_{5/3}\Delta_{1/3}]O_4$, where ( ) denotes tetrahedral sites, [ ] octahedral sites and $\Delta$ vacancies. Besides its importance in processes concerning the exsolution and oxidation of titanomagnetite in geochemistry and paleomagnetism [1–4], it has attracted attention because of its application in magnetic tape recording materials [5]. Although the doping of the material by metals such as trivalent aluminium [6, 7], magnesium, and gadolinium [8] (and also by cobalt and nickel to improve the magnetic performance [9]) has been of interest for some years, there appears to be a sparcity of data concerning doping by tetravalent metals such as tin or titanium. Such data are of great interest, because of the occurrence of titanomaghemite in nature [1–4], and because substitution of tetravalent ions can be used to stabilize $\gamma$-$Fe_2O_3$ against transformation to $\alpha$-$Fe_2O_3$ (hematite) at elevated temperatures [10].

  

The most important question associated with the structural and physical properties of these materials concerns the occupation by the dopant of either the tetrahedral, or octahedral sites and its influence on magnetization. We report here on the preparation of tin- and titanium-doped $\gamma$-$Fe_2O_3$ and the investigation of the local coordination of the dopant ions and the magnetic properties by a range of techniques including $^{57}$Fe- and $^{119}$Sn-Mössbauer spectroscopy. $^{57}$Fe Mössbauer spectra recorded at low temperature in the presence of an applied magnetic field enable an estimation of the site occupation and the effect of the dopant on the canting angles.

## 2. Experimental details

$\gamma$-$Fe_2O_3$ and the tin- and titanium-doped variants were prepared as previously described [10] by adding aqueous ammonia to aqueous mixtures of 2/3 iron(III) chloride hexahydrate, 1/3 iron(II) chloride tetrahydrate and, in the case of tin- and titanium-doped compounds, either tin(II) chloride or titanium(IV) chloride until pH7. The mixtures were boiled under reflux (3 h). The precipitates were removed by filtration, washed with 95% ethanol until no chloride ions could be detected in the washings by silver nitrate solution, and heated in air at 250 °C for 12 h.

X-ray powder diffraction data were recorded with a Siemens D5000 diffractometer in reflection mode using Cu–$K_\alpha$ radiation. The $^{57}$Fe Mössbauer spectra were recorded at 4.2, 77 and 298 K with a conventional constant acceleration spectrometer in transmission geometry using a 400 MBq $^{57}$Co/Rh source. All the isomer shift data are reported relative to that of $\alpha$-iron at room temperature. $^{57}$Fe Mössbauer spectra were also recorded in the presence of an applied field using a cryomagnetic device where the applied field is oriented parallel to the beam of the $\gamma$-rays. $^{119}$Sn Mössbauer spectra were recorded at 298 and 17 K with a conventional constant acceleration spectrometer in transmission geometry and a 200 MBq $Ba^{119m}SnO_3$ source. The isomer shifts are given relative to that of $\alpha$-iron at room temperature. Electron micrographs were recorded from specimens suspended on copper grids using a JEOL 2000 FX transmission electron microscope with an accelerating voltage of 200 keV.

The Sn K- and Ti-K-edge-x-ray absorption spectra were obtained at the SRS at the Daresbury Laboratory in single-bunch mode. The ring current varied between 25 and 15 mA in the 2 GeV storage ring. Station 9.2 was used to collect the tin K-edge data using a Si(220) double crystal monochromator which was detuned by 40% to remove higher order harmonics. The monochromator was calibrated with tin foil, the edge of which was taken to be at 29 195 eV. The titanium K-edge data were collected on Station 8.1 with a Si(111) double-crystal monochromator detuned by 50%. Calibration was achieved with a titanium foil with an edge position taken to be 4965 eV. Data were collected in transmission mode using ion chambers filled with noble gases. The ground samples were sprinkled onto adhesive tape, using three layers of tape for the titanium-containing sample and eight layers for the tin-containing sample and, for both samples, four sets of data were collected and averaged to improve the signal-to-noise ratio.

The data were reduced using the SRS programs EXCALIB and EXBROOK. EXAFS data analyses were performed using the program EXCURV98 [11]. Phaseshifts were calculated *ab initio* using Hedin–Lundqvist exchange potentials and von Barth ground state potentials. The refinement was performed using single scattering with coordination numbers fixed from the iron sites in $\gamma$-$Fe_2O_3$. The shell radii were allowed to vary in the fitting process. The fit index $R$ quoted in table 1 is defined by

$$R = \Sigma_i[(1/(\sigma_i))(|\text{experiment(i)} - \text{theory(i)}|] * 100\% \tag{1}$$

where $1/(\sigma_i) = [k(i)]^3/(\Sigma_i[k(i)]^3|\text{experiment(i)}|)$ [11].

**Table 1.** Best-fit parameters for tin K- and titanium K-edge EXAFS recorded from 8% tin- and titanium-doped $\gamma$-$Fe_2O_3$ at 298 K and the sites for Fe2 (for Sn) and Fe4 (for Ti) as calculated from the diffraction data.

| Atom type | Number of atoms | Distance (Å)[a] | $2\sigma^2$(Å$^2$)[b] | Number of atoms (from diffraction) | Distance (from diffraction) (Å) | Mean distance (from diffraction) (Å)[c] |
|---|---|---|---|---|---|---|
| Sn-doped $\gamma$-$Fe_2O_3$ ($R = 28.3$) | | | | | | |
| O | 6 | 2.05 | 0.014 | 2 | 1.988 | 2.04 |
| O | | | | 2 | 2.043 | |
| O | | | | 2 | 2.090 | |
| Fe | 4.66 | 3.10 | 0.020 | 2 | 2.984 | 3.01 |
| Fe | | | | 2 | 3.025 | |
| Fe | | | | 0.66 | 3.026 | |
| Fe | 6 | 3.47 | 0.031 | 2 | 3.460 | 3.47 |
| Fe | | | | 2 | 3.466 | |
| Fe | | | | 2 | 3.472 | |
| Ti-doped $\gamma$-$Fe_2O_3$ ($R = 38.2$) | | | | | | |
| O | 4 | 1.94 | 0.017 | 2 | 1.997 | 2.02 |
| O | | | | 2 | 2.053 | |
| O | 2 | 2.30 | 0.017 | 2 | 2.342 | 2.34 |
| Fe | 2 | 2.69 | 0.043 | 2 | 2.716 | 2.72 |
| Fe | 4 | 3.06 | 0.029 | 2 | 2.966 | 2.99 |
| Fe | | | | 2 | 3.011 | |

[a] $\pm 1\%$.
[b] $\pm 4\%$.
[c] $\pm 0.01$.

## 3. Results and discussion

### *3.1. XRD and EXAFS*

The x-ray powder diffraction patterns showed all the materials to be single phase with $\gamma$-$Fe_2O_3$-related structures. In marked contrast to the refinement for tin-doped $Fe_3O_4$ [10], x-ray powder diffraction was unable to yield definitive support for the substitution of tin into the structure of $\gamma$-$Fe_2O_3$. The electron micrographs yielded average particle sizes of the order of 20 nm.

The fitting of the tin- and titanium-K-edge EXAFS was based on the structure of $\gamma$-$Fe_2O_3$ [12] which contains one tetrahedral iron site designated here as Fe1 and three octahedral iron sites. Two of the octahedral iron sites (designated as Fe2 and Fe3) are fully occupied whilst the third (designated as Fe4) is $\frac{1}{3}$ occupied. The results of the EXAFS analyses are shown in table 1 and figure 1 shows the Sn K-edge EXAFS. Table 1 also details the atomic neighbours calculated from the diffraction data for the sites, which best match the EXAFS data.

The occupation by the dopant of each of the four sites was considered as a starting model using appropriate groupings of Debye–Waller factors. Oxygen atoms not in the first coordination sphere were ignored and are not listed in table 1. The fitting of the tin K-edge data was best achieved by considering models in which tin substituted for iron on sites Fe2 or Fe3. Models based on substitution of either of these sites resulted in similar fit indices. However, for site Fe2 only three shells were needed for a satisfactory fit, while site Fe3 required five shells, hence the fit for site Fe2 is statistically much better. The iron atoms in the second coordination

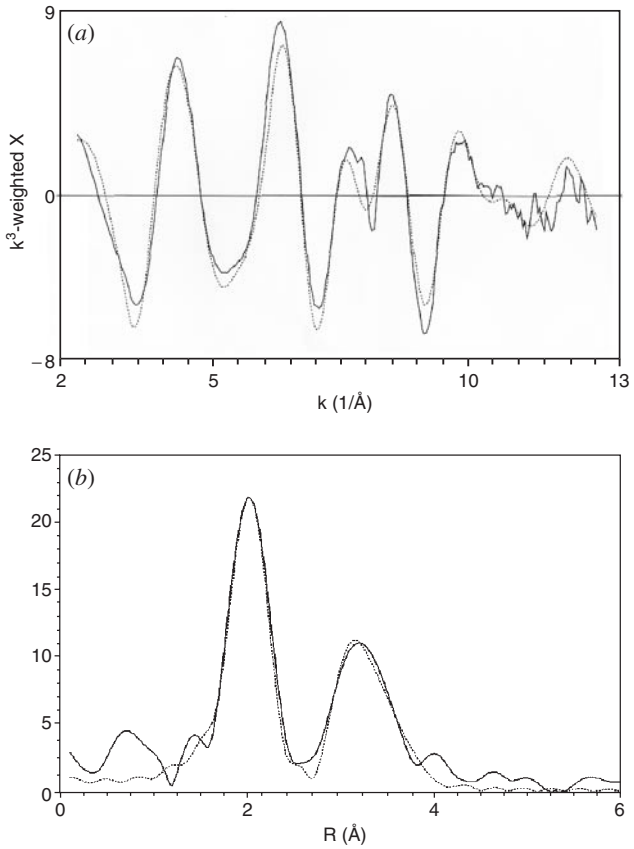


**Figure 1.** (*a*) Tin $k^3$-EXAFS recorded from tin-doped $\gamma$-$Fe_2O_3$(—— experimental, – – – theoretical). (*b*) Phase shifted Fourier transform of tin $k^3$-EXAFS of tin-doped $\gamma$-$Fe_2O_3$(—— experimental, – – – theoretical).

sphere are at a slightly longer distance 3.10 Å than diffraction results would indicate (3.01 Å) but this may be due to some local distortion in the structure around the sites where tin is located. Thus the tin K-edge EXAFS strongly suggests that tin is located mainly in the fully occupied octahedral site Fe2, though partial occupation of the Fe3 site cannot be ruled out. Models based on the other two iron sites Fe1 and Fe4 failed to produce adequate fits to the EXAFS data.

The Ti K-edge EXAFS data (figure 2) suggest that titanium has a split first coordination sphere of oxygen atoms containing four short- and two long-Ti–O bonds. The other two shells (two Fe at 2.69 Å and four Fe at 3.06 Å) that are statistically significant are consistent with titanium being located on the partially occupied octahedral Fe4 site. In this site further iron shells might be expected at *ca.* 3.36 and 3.51 Å but the addition of these shells to the model did not improve the fit. The results suggest that the titanium is mainly located on site Fe4 but that some fraction is situated elsewhere. Attempts to add extra shells to the model that represented other possible sites did not improve the fit. Thus the EXAFS analysis suggests that titanium is disordered over the partially occupied Fe4 site.

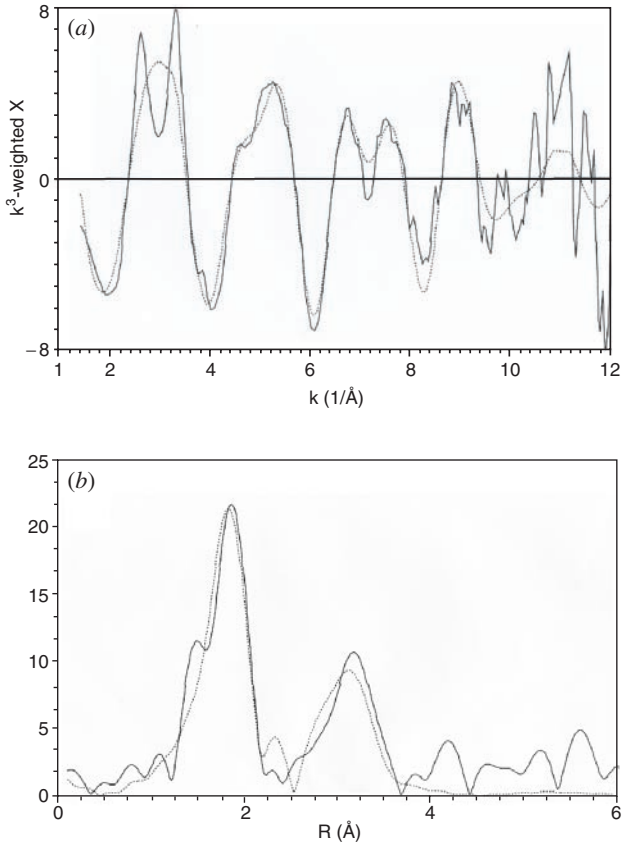


**Figure 2.** (*a*) Titanium $k^3$-EXAFS recorded from titanium-doped $\gamma$-$Fe_2O_3$ (—— experimental, – – – theoretical). (*b*) Phase shifted Fourier transform of titanium $k^3$-EXAFS recorded from titanium-doped $\gamma$-$Fe_2O_3$ (—— experimental, – – – theoretical).

### *3.2.* $^{57}$*Fe Mössbauer spectroscopy*

The $^{57}$Fe Mössbauer spectra recorded at 298 K from pure $\gamma$-$Fe_2O_3$ and from $\gamma$-$Fe_2O_3$ doped with 2.5% tin, 8% tin, and 8% titanium are shown in figure 3. The spectra recorded from undoped $\gamma$-$Fe_2O_3$ and 2.5% tin-doped $\gamma$-$Fe_2O_3$ can be satisfactorily fitted to sextets with narrow line widths or narrow field distributions with zero quadrupole shift and an isomer shift of $\sim$0.32 mm s$^{-1}$ characteristic of $\gamma$-$Fe_2O_3$. In the case of 8% tin- and titanium-doped $\gamma$-$Fe_2O_3$ a doublet, characteristic of $Fe^{3+}$, was also needed to successfully fit the spectra at room temperature. No divalent iron component was detected. The application of an external field of 0.7 T perpendicular to the gamma rays caused the doublet to virtually disappear in the spectrum recorded from tin-doped $\gamma$-$Fe_2O_3$ and to be considerably diminished in the spectrum recorded from the titanium doped-sample. These results indicate that iron is partially present in a superparamagnetic state in the two samples at room temperature. This conclusion is confirmed by the spectra recorded at 77 and at 4.2 K (figure 4) from all four samples which can be fitted with two sextets with slightly different isomer shift, the same quadrupole shift, and which are consistent with the presence of both tetrahedral and octahedral iron sites. The main hyperfine parameters for the discrete sextets and doublets are given in table 2.

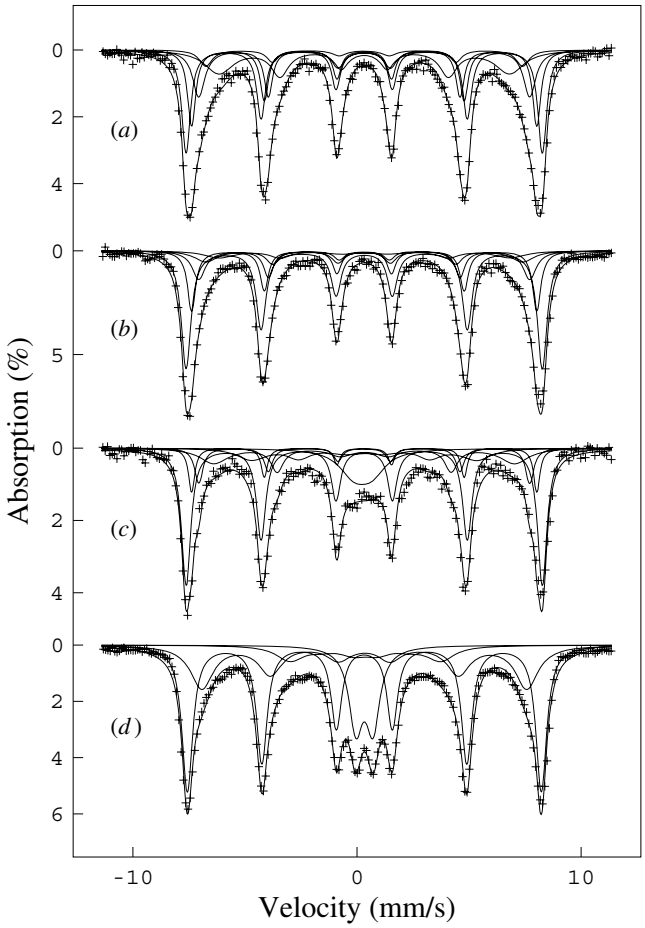


**Figure 3.** $^{57}$Fe Mössbauer spectra recorded at 298 K; (*a*) $\gamma$-$Fe_2O_3$, (*b*) 2.5% tin-doped $\gamma$-$Fe_2O_3$, (*c*) 8% tin-doped $\gamma$-$Fe_2O_3$ and (*d*) 8% titanium-doped $\gamma$-$Fe_2O_3$.

To examine the effect of the dopant, $^{57}$Fe Mössbauer spectra were recorded from all four samples at 10 K in an external magnetic field of 6 T parallel to the direction of the gamma ray beam. The spectra recorded from the doped samples are shown in figure 5. A splitting of the outermost lines 1 and 6 is clearly evident and a significant decrease in the intensity of lines 2 and 5 is observed. The spectra can be fitted with two discrete distributions of the hyperfine field corresponding to the octahedral and tetrahedral iron sites. Within each distribution the isomer shift and the quadrupole shift were considered to be identical for all sextets. The isomer shifts for the two distributions differ by approximately 0.1 mm $s^{-1}$ in all samples, which is consistent with the difference usually observed in these types of oxides. The dips at the positions of lines 2 and 5 indicate a non-vanishing component of the hyperfine field perpendicular to the applied field. The ratio of the areas of the lines (2, 5) to the lines (1, 6) is related to the canting angle between the hyperfine field and the external field [6, 13, 14]. Indeed, the effective field $\boldsymbol{B}_{\rm eff}$ at the iron nucleus results from the vector sum of the hyperfine field $\boldsymbol{B}_{\rm hf}$ and the applied field $\boldsymbol{B}_{\rm app}$. If $\boldsymbol{B}_{\rm eff}$ is inclined at an angle $\vartheta$ from the gamma-ray direction, the line areas are in the ratio $3{:}2p{:}1{:}1{:}2p{:}3$ with $p = 2\sin^2\vartheta/(1{+}\cos^2\vartheta)$. By normalizing the total area $\Sigma A_{i,7-i} = 1$,

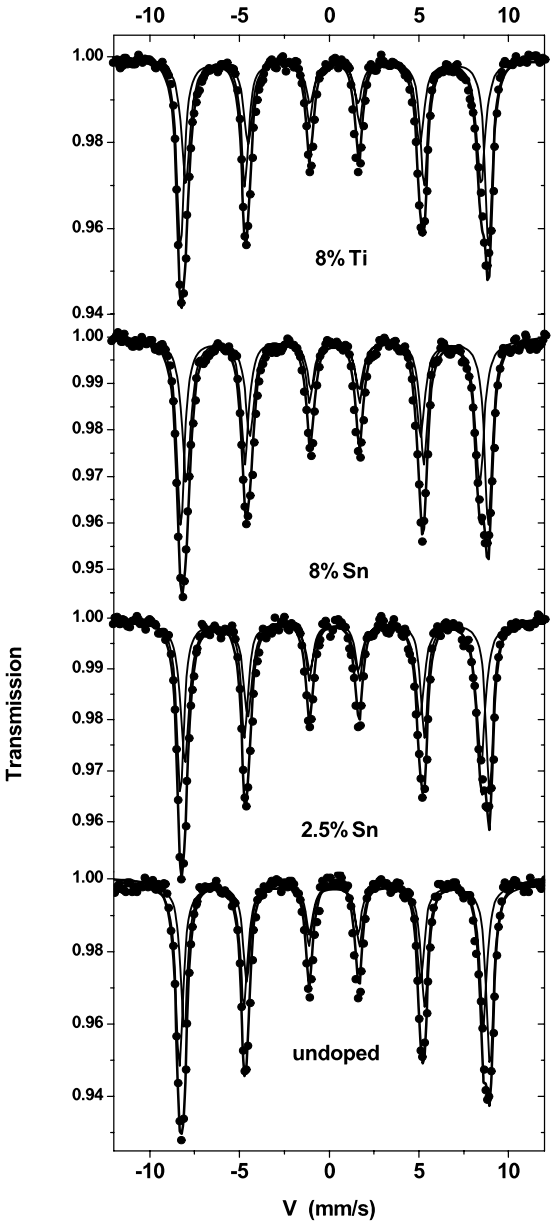


**Figure 4.** $^{57}$Fe Mössbauer spectra recorded at 4.2 K from 8% titanium-, 8% tin-, 2.5% tin-doped $\gamma$-$Fe_2O_3$ and undoped $\gamma$-$Fe_2O_3$.

the area of each of the lines 2, 5 is $A_{2,5} = 1/4 \sin^2 \vartheta$. The values of the mean hyperfine field at the octahedral and tetrahedral sites can be estimated from those of the in-field effective field using the following relationship:

$$\langle B_{\mathrm{hf}}^2 \rangle = \langle B_{\mathrm{eff}}^2 \rangle + B_{\mathrm{app}}^2 - 2^* \langle B_{\mathrm{eff}} \rangle^* B_{\mathrm{app}}{}^* \cos\langle \vartheta \rangle \tag{2}$$

where the angle $\langle \vartheta \rangle$ defines the direction of the mean effective field with respect to the gamma ray direction.

Within each distribution, the angle $\vartheta$, which defines the direction of the effective field with respect to the gamma ray direction, i.e. the applied field direction, was assumed free during

**Table 2.** $^{57}$Fe Mössbauer parameters recorded at 298 and 4.2 K.

| Sample | T(K) | Spectral component | $\delta$ (mm s$^{-1}$) (±0.01) | $\Delta$ or $2\varepsilon$ (mm s$^{-1}$) (±0.01) | $B_{hf}$ (T) (±0.2) | Area ratio % (±2) |
|---|---|---|---|---|---|---|
| | 298 | 'The main sextet' | 0.33 | 0.01 | 47.3 | |
| Maghemite | | Octahedral | 0.47 | 0.03 | 53.4 | 56 |
| | 4.2 | Tetrahedral | 0.42 | 0 | 51.5 | 44 |
| | 298 | 'The main sextet' | 0.32 | −0.01 | 48.1 | |
| 2.5% Sn | | Octahedral | 0.47 | 0.03 | 53.2 | 50 |
| | 4.2 | Tetrahedral | 0.40 | −0.05 | 50.9 | 50 |
| | | 'The main sextet' | 0.32 | 0 | 46.2 | 89 |
| 8% Sn | 298 | The doublet | 0.30 | 0.75 | | 11 |
| | | Octahedral | 0.48 | 0 | 52.9 | 53 |
| | 4.2 | Tetrahedral | 0.43 | −0.12 | 50.5 | 47 |
| | | 'The main sextet' | 0.34 | 0 | 45.8 | 85 |
| 8% Ti | 298 | The doublet | 0.33 | 0.76 | | 15 |
| | | Octahedral | 0.46 | 0.03 | 53 | 56 |
| | 4.2 | Tetrahedral | 0.42 | −0.03 | 50.8 | 44 |

**Table 3.** $^{57}$Fe Mössbauer parameters calculated from the spectra recorded at 10 K in an external magnetic field of 6 T parallel to the $\gamma$-rays.

| Sample | Sextet | $\delta$ (mm s$^{-1}$) (±0.01) | $\Delta$ or $2\varepsilon$ (mm s$^{-1}$) (±0.01) | $B_{eff}$ (T) (±0.2) | Area ratio % (±2) | Canting angle $\langle\vartheta\rangle$ (±5) | $B_{hf}$ (T) (±0.3) |
|---|---|---|---|---|---|---|---|
| Maghemíte | Octahedral | 0.51 | 0 | 47.9 | 60 | 23 | 53.5 |
| | Tetrahedral | 0.40 | −0.09 | 58 | 40 | 12 | 52.4 |
| 2.5 % Sn | Octahedral | 0.52 | −0.01 | 48 | 58 | 35 | 53.0 |
| | Tetrahedral | 0.42 | −0.11 | 57.4 | 42 | 15 | 51.6 |
| 8% Sn | Octahedral | 0.52 | −0.14 | 47.8 | 52 | 30 | 53.1 |
| | Tetrahedral | 0.42 | −0.06 | 56.2 | 48 | 35 | 51.4 |
| 8% Ti | Octahedral | 0.51 | 0 | 47.9 | 52 | 32 | 53.1 |
| | Tetrahedral | 0.41 | −0.08 | 57.8 | 48 | 18 | 52.1 |

the fitting procedure. The distributions enable an average value of both $\langle B_{eff}\rangle$ and $\langle\vartheta\rangle$ to be independently estimated, for the tetrahedral and octahedral components and the results are shown in tables 3 and 4. The results show a good agreement between the values of the angles and their corresponding effective field in comparison to the hyperfine field. For example, for the tetrahedral iron site, the effective field corresponding to iron moments oriented antiparallel to the applied field is associated with the small value of $\vartheta$, (i.e. $B_{eff} = B_{hf} + B_{app}$), while the lowest effective fields are associated with an angle $\vartheta$ close to 90° which is consistent with large canting. However, the main fitting difficulty remains with the estimate of the limits of the distribution, especially the lower limit of the tetrahedral component and the higher limit of the octahedral component. The results from the fitting of the spectra and the calculation of the mean angle $\vartheta$ are collected in table 3.

The effect of the dopants on the magnetic ordering in maghemite was further examined by recording a series of $^{57}$Fe Mössbauer spectra from the 8% tin-doped sample at 10 K in external magnetic fields between 2 and 8 T. The spectra are shown in figure 6 and the hyperfine parameters are collected in table 4.

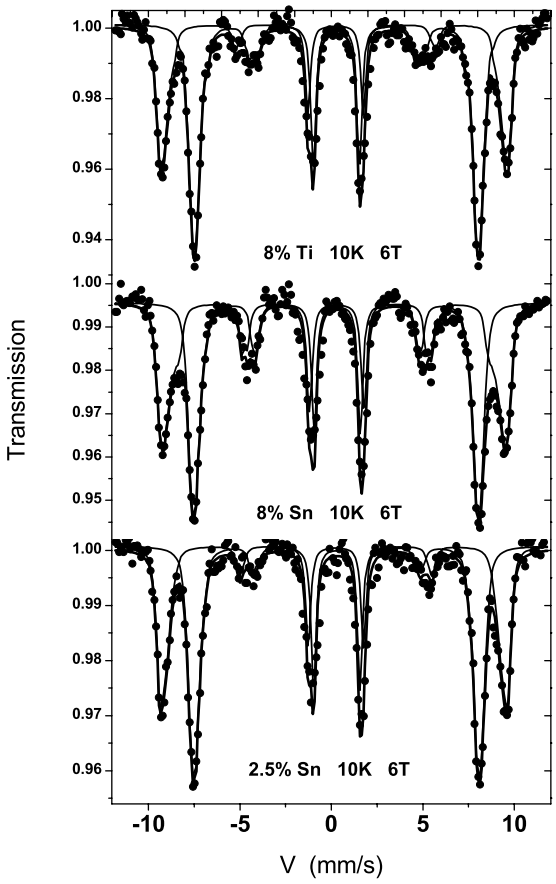


**Figure 5.** $^{57}$Fe Mössbauer spectra recorded from 8% titanium-, 8% tin- and 2.5% tin-doped $\gamma$-$Fe_2O_3$ at 10 K in an external magnetic field of 6 T parallel to the gamma rays.

**Table 4.** $^{57}$Fe Mössbauer parameters for 8% tin-doped $\gamma$-$Fe_2O_3$, calculated from the series of spectra recorded at 10 K in an external magnetic field of 2–8 T parallel to the $\gamma$-rays.

| Applied field (T) | Sextet | $\delta$ (mm s$^{-1}$) (±0.01) | $\Delta$ or $2\varepsilon$ (mm s$^{-1}$) (±0.01) | $B_{\text{eff}}$ (T) | Area ratio % (±2) | Canting angle $\langle\vartheta\rangle$ (±5) | $B_{\text{hf}}$ (T) |
|---|---|---|---|---|---|---|---|
| 2 | Octahedral | 0.53 | −0.13 | 50.7 (5) | 57 | 36 | 52.3 (6) |
| | Tetrahedral | 0.43 | 0.02 | 53.0 (5) | 43 | 36 | 51.4 (6) |
| 4 | Octahedral | 0.53 | −0.13 | 49.2 (4) | 54 | 37 | 52.4 (5) |
| | Tetrahedral | 0.41 | −0.07 | 54.5 (4) | 46 | 31 | 51.1 (5) |
| 6 | Octahedral | 0.52 | −0.14 | 47.8 (2) | 52 | 30 | 53.1 (3) |
| | Tetrahedral | 0.42 | −0.06 | 56.2 (2) | 48 | 35 | 51.4 (3) |
| 8 | Octahedral | 0.52 | −0.14 | 46.3 (2) | 54 | 34 | 53.1 (3) |
| | Tetrahedral | 0.45 | −0.04 | 58.0 (2) | 46 | 35 | 51.6 (3) |

It is important to emphasize that the higher the external field, the better will be the resolution and more accurate the effective field value. As shown in table 4, the hyperfine field values for the 8% tin-doped $\gamma$-$Fe_2O_3$ are estimated as ∼53.1 and ∼51.5 T regardless of the magnitude of the external field. It can therefore be deduced that the hyperfine fields, at both tetrahedral and octahedral iron sites, undergo a small decrease when the content of the dopant increases.

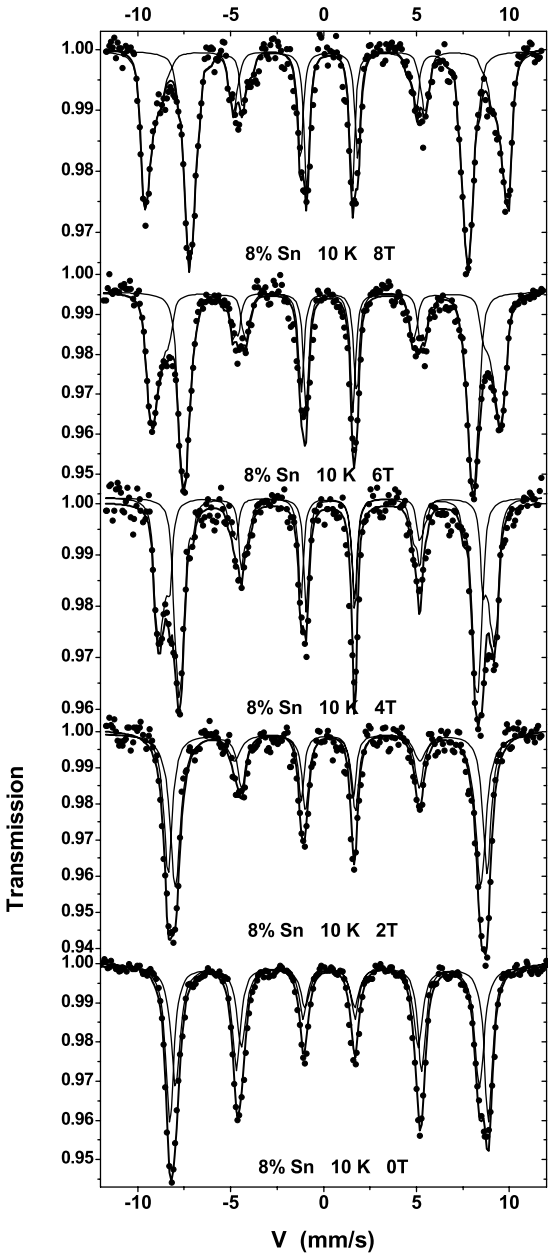


**Figure 6.** $^{57}$Fe Mössbauer spectra recorded at 10 K from 8% tin-doped $\gamma$-$Fe_2O_3$ in an external magnetic field of 2–8 T parallel to the gamma rays.

The effect of the doping on the area ratio can be estimated from the applied field measurement. For pure $\gamma$-$Fe_2O_3$, 60% of the area can be assigned to the sextet corresponding to iron in octahedral sites and 40% to the sextet corresponding to iron in tetrahedral sites. This is in reasonable agreement with the $5/3$ area ratio expected from the structure of pure $\gamma$-$Fe_2O_3$. If tin preferentially substitutes for iron in the octahedral site, this ratio should decrease with

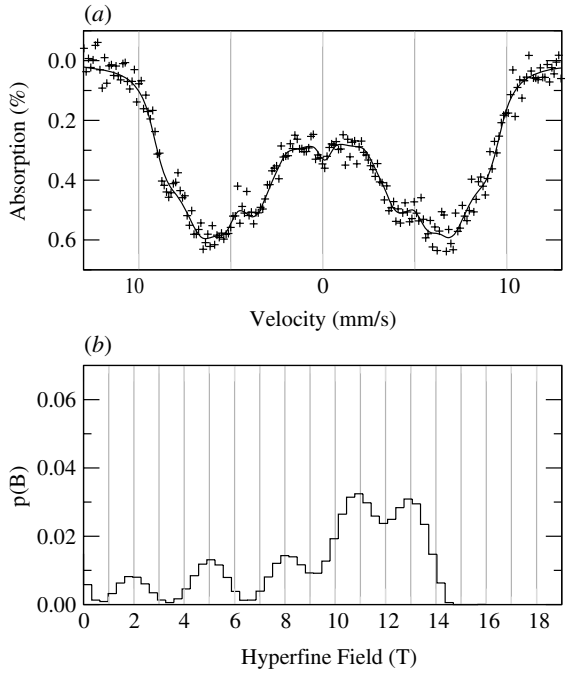


**Figure 7.** (*a*) $^{119}$Sn Mössbauer spectrum recorded at 298 K from 2.5% tin-doped $\gamma$-$Fe_2O_3$. (*b*) The magnetic hyperfine field distribution for 2.5% tin-doped $\gamma$-$Fe_2O_3$ calculated from the Mössbauer spectrum recorded at 298 K.

increasing amounts of tin-doping. This is confirmed by the decrease in area ratio from 58/42 for 2.5% tin doped $\gamma$-$Fe_2O_3$ to 52/48 for the 8% sample, which is in reasonable agreement with theoretical values, 59/41 and 56/44, respectively. Similar behaviour is observed for titanium-doped maghemite, for which the same ratio is obtained from in-field Mössbauer experiments (table 3).

### *3.3. $^{119}$Sn Mössbauer spectroscopy*

Figure 7(*a*) shows the $^{119}$Sn Mössbauer spectrum recorded at room temperature from 2.5% tin-doped $\gamma$-$Fe_2O_3$. Although the $Sn^{4+}$ ion itself is non-magnetic, its nucleus can sense a non-vanishing magnetic hyperfine field by the effect of super-transferred hyperfine interaction (STHI) with the magnetically ordered $Fe^{3+}$ in the $\gamma$-$Fe_2O_3$ structure. The magnetic splitting of the $^{119}$Sn spectra gives unambiguous evidence for the substitution of the tin into the $\gamma$-$Fe_2O_3$ lattice. Three sextets with broad lines (and nearly zero quadrupole shift) and a doublet (with an isomer shift of 0.15 mm $s^{-1}$ and quadrupole splitting of 0.56 mm/ characteristic of $SnO_2$) were needed to obtain a reasonable fit to the data. The result indicates that fitting the spectrum to a distribution of hyperfine magnetic fields is more appropriate. Hence the spectra were fitted without a doublet component to a model-independent distribution of the magnetic hyperfine fields [15]. The sextets of the field distributions were constrained to an area ratio of 3:2:1. All the line widths of the sextets were kept fixed (0.9 mm $s^{-1}$) in the fitting procedure and the isomer shifts were allowed to vary linearly with the magnetic hyperfine field, but the quadrupole shifts were kept constant (zero) in the final version of the fitting. The magnetic field distribution for the 2.5% tin-doped $\gamma$-$Fe_2O_3$ is shown in figure 7(*b*). This field distribution

shows that only a negligible part (less than 5%) of the tin can be present as $SnO_2$ in the sample although the field distribution cannot distinguish between a contribution from the doublet of tin dioxide and components with magnetic hyperfine fields less than 1–2 T. In the case of the 8% tin-doped $\gamma$-$Fe_2O_3$, up to 10% of the distribution is within such a region. The spectra recorded from both samples showed (i) a broad asymmetric maximum in the field distribution at about 12 T, (ii) identical structure between 4 and 9 T with small maxima at 5 and 8 T. In testing the reality of the two maxima, two changes in the fitting procedure were tried. Firstly, the 1:2:3 constraint was released. Small statistical improvements were obtained for a ratio of 1:1.8−1.9:2.7, but without a significant change in the area or position of the peaks at 5 and 8 T. Secondly, a smoothing parameter in the distribution program [15] was allowed to increase and smear out the peaks. If the maxima were a result of artefacts, no changes would be expected in the $\chi^2$ value. Application of this test showed $\chi^2$ to increase, supporting the reality of the two peaks at 5 and 8 T. Compared to earlier work on tin-doped magnetite, $Fe_3O_4$ [16], the field distribution for tin-doped $\gamma$-$Fe_2O_3$ is more complex. In spite of the same structure and similar magnetic hyperfine field at the iron nucleus in $\gamma$-$Fe_2O_3$ and $Fe_3O_4$, the maximum hyperfine field at the $Sn^{4+}$ ions in $\gamma$-$Fe_2O_3$ is only about 2/3 of that observed in $Fe_3O_4$ (21 T). The complexity in the distribution of the magnetic sextets may be due to different vacancy ordering in the $\gamma$-$Fe_2O_3$ structure resulting from the location of $Sn^{4+}$ ions on octahedral sites.

## 4. Conclusion

The results recorded from $^{57}$Fe Mössbauer spectroscopy from tin- and titanium-doped $\gamma$-$Fe_2O_3$ in an external magnetic field of 2 to 8 T and from EXAFS show that tin and titanium occupy the octahedral as opposed to tetrahedral sites in $\gamma$-$Fe_2O_3$. The EXAFS shows that different iron sites are occupied by tin and titanium. The hyperfine field values at both tetrahedral and octahedral iron sites decrease slightly when the dopant content increases. The canting angle for both sublattices in $\gamma$-$Fe_2O_3$ were determined from the in-field Mössbauer spectra and, in the case of doping with tin, an increase of the canting angle was detected. The $^{119}$Sn Mössbauer spectra show that the maximum hyperfine field seen by the $Sn^{4+}$ ions in $\gamma$-$Fe_2O_3$ is only about 2/3 of that observed in $Fe_3O_4$ and, in spite of the same structure, the field distribution is more complex.

## Acknowledgment

We wish to acknowledge the use of the EPSRC's Chemical Database Service at Daresbury Laboratory.

## References

[1] Vandenberghe R E and De Grave E 1989 Mössbauer effect studies of oxidic spinels *Mössbauer Spectroscopy Applied to Inorganic Chemistry* vol 3, ed G J Long and F Grandjean (New York: Plenum) pp 59–182
[2] Moukarika A, O'Brian F and Coey J M D 1991 *Geophys. Res. Lett.* **18** 2043–6
[3] Resende M, Allan J and Coey J M D 1986 *Earth Planet. Sci. Lett.* **78** 322
[4] Steinthorsson S, Helgason Ö, Madsen M B, Bender Koch C, Bentzon M D and Mørup S 1992 *Mineral. Mag.* **56** 185–99
[5] Pollard R J 1988 *Hyperfine Interact.* **41** 509–12
[6] Da Costa G M, De Grave E, Bowen L H, Vandenberghe R E and De Bakker P M A 1994 *Clay and Clay Minerals* **42** 628–33
[7] Da Costa G M, De Grave E and Vandenberghe R E 1998 *Hyperfine Interact.* **117** 207–43
[8] Anamtharaman M R, Malini K A, Sindhu P D, Sindhu S and Keer H V 1999 *Ind. J. Pure Appl. Phys.* **37** 842–7

[9] Anamtharaman M R, Scsham K, Shringi S N and Keer H V 1981 *Bull. Mater. Sci.* **6** 59
[10] Berry F J, Greaves C, Helgason Ö and McManus J 1999 *J. Mater. Chem.* **9** 223–6
[11] Binsted N, Campbell J W, Gurman S J, Ross I and Stephenson P C 1998 *Excurv98 (CCLRC Daresbury Laboratory Computer Program)*
[12] Fletcher D A, McMeeking R F and Parkin D 1996 *J. Chem. Inf. Comput. Sci.* **36** 746–9
[13] Tronc E, Prené P, Jolivet J P, Dormann J L and Greneche J M 1998 *Hyperfine Interact.* **112** 97–100
[14] Morales M P, Serna C J, Bødker F and Mørup S 1997 *J. Phys.: Condens. Matter* **9** 5461–7
[15] Wivel C and Mørup S 1981 *J. Phys. E: Sci. Instrum.* **14** 605
[16] Berry F J, Helgason Ö, Jónsson K and Skinner S J 1996 *J. Solid State Chem.* **122** 353